Eom *et al. Int J Concr Struct Mater* (2019) 13:1
https://doi.org/10.1186/s40069-018-0311-2

International Journal of Concrete Structures and Materials

RESEARCH Open Access

Behavior and Design of Distributed Belt Walls as Virtual Outriggers for Concrete High-Rise Buildings

Tae-Sung Eom[1*], Hiubalt Murmu[2] and Weijian Yi[3]

Abstract

A new lateral force-resisting structural system for concrete high-rise buildings, distributed belt wall system, is proposed. Unlike conventional belt structures, the belt walls infilling the space between perimeter columns are distributed separately along the overall building height. In this study, the force transfer mechanism and performance of the distributed belt walls, acting as virtual outriggers under lateral load, are investigated. For the reinforcement of the belt walls subjected to high shear demand, a reinforcing method using high-strength prestressing strands (i.e. PSC belt wall) is suggested, and the shear strength of the PSC belt walls is estimated based on the compression field theory. By performing nonlinear finite element analysis, the shear behavior of the PSC belt walls, including cracking and yield strengths, is investigated in detail. Based on these investigations, recommendations for the shear design of the belt walls reinforced by high-strength prestressing strands are given.

Keywords: belt wall, outrigger, shear design, prestressed concrete, compression field theory, lateral force-resisting system, high-rise building

1 Introduction

In high-rise buildings subjected to lateral loads such as wind and earthquake, outrigger structures connecting the perimeter columns to the core wall have been traditionally used to reduce lateral drift. By converting bending moment acting in the core wall into axial tension and compression forces of the perimeter columns, the outrigger contributes to reduction in the lateral drift at the top floor of the building. In addition, if the perimeter columns are tied by a strong belt structure, the outrigger effect can spread over the adjacent columns to which the outrigger is not directly connected. However, as shown in Fig. 1a, the conventional outrigger system has disadvantages in architectural planning, due to interference with space planning at the floor where the outrigger members are installed.

To overcome such disadvantages, alternative outrigger systems such as the offset outrigger and virtual outrigger have been studied (Stafford Smith et al. 1996; Nair 1998; Dean et al. 2001; Choi and Joseph 2012; Eom et al. 2013). As shown in Fig. 1b, in such alterative outrigger systems, the conventional outriggers connecting directly the core wall with the perimeter columns are not used. Instead, only belt structures to tie the adjacent perimeter columns are used. Although the core wall is not connected directly with the perimeter columns, a portion of the horizontal shear force acting on the core wall is transferred to the belt structures through the upper (or lower) floor slab, and the shear force is returned to the core wall through the lower (or upper) floor slab. Through this process, axial tension and compression forces are induced in the perimeter columns tied to the belt structures, while the bending moment acting on the core wall is reduced (Nair 1998).

Currently, the outrigger and belt structures carrying large forces are mostly constructed by steel or steel–concrete composite trusses, while the core walls are often constructed by reinforce concrete (see Fig. 2). In

*Correspondence: tseom@dankook.ac.kr
[1] Dept. of Architectural Engineering, Dankook Univ., 152 Jukjeon-ro, Yongin-si, Gyeonggi-do 448-701, South Korea
Full list of author information is available at the end of the article
Journal information: ISSN 1976-0485 / eISSN 2234-1315

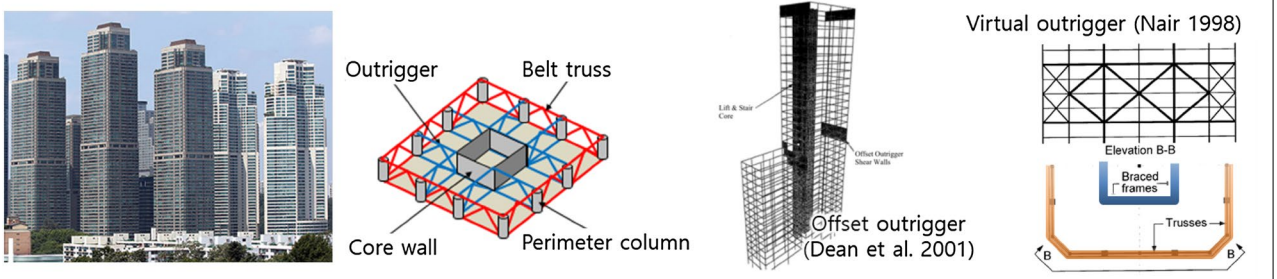

a **Conventional core wall-outrigger-belt truss system** **b** **Alternative outrigger systems**

Fig. 1 Conventional and alternative outrigger systems for high-rise buildings.

Fig. 2 Mixed construction of steel outrigger and belt trusses and reinforced concrete core wall and columns.

this case, overall construction period can increase due to interference between the steel construction process of the outrigger and belt trusses and the concrete construction process of the core walls. Furthermore, structural details at the connection where the outrigger members are joined to the core wall are complicated. This is also the same for the connection to the perimeter columns constructed by reinforced concrete. On the other hand, if concrete walls can be used as the outrigger and belt structures, complicated connection details might be avoided, and construction period and cost might be also reduced because interference between the construction processes is minimized.

Thus, a new lateral force-resisting system for concrete high-rise buildings, distributed belt wall system, is proposed in this study. In the distributed belt wall system, first, belt walls are used without outrigger, and thus they contributes to the lateral force resistance of the building by acting as virtual outriggers (Stafford Smith et al. 1996; Nair 1998). Second, by distributing the belt walls over the building height, instead of concentrating at a specific floor, such as the mid-height and roof, space loss at the floor where outrigger and/or belt structures are installed is minimized. Third, in the constructional viewpoint, by using concrete belt walls, it is possible to minimize interference with the concrete construction process of the adjacent perimeter columns and core walls.

The behavior and design method of the distributed belt wall system are studied as follows. By performing a parametric study, the force transfer mechanism and lateral drift-decreasing performance of the distributed belt walls acting as virtual outriggers are investigated. In addition, considering high shear demand in the distributed belt walls, a reinforcing method using high-strength prestressing strands is proposed and the belt wall shear strengths at cracking and strand yielding are estimated, based on the compression field theory. Finally, the shear behavior of the prestressed concrete belt walls such as concrete cracking and post-cracking behavior is verified by performing nonlinear finite element analysis.

2 Distributed Belt Wall Structure System

In this section, the force transfer mechanism of the conventional belt wall system (i.e. concentrated belt wall system) and proposed distributed belt wall system are investigated through parametric study. For the parametric study, a commercial structural analysis and design software, MIDAS/GEN, was used (MIDAS IT 2006).

2.1 Concentrated Belt Wall System

Figure 3 shows a 30-story prototype concrete buildings. The story height is 4 m and the floor plan is a square of length 54 m. At the center of the floor plan, two C-shaped core walls, each of which is 18 m long and 6 m wide (thickness 300 mm), are used. Along the perimeter, 24 columns of 800 mm × 800 mm in section size are placed at a spacing of 9 m. The perimeter columns are tied by the spandrel beams of section 400 mm × 600 mm. As shown in Fig. 3, as the lateral force-resisting system, four conventional structural systems are considered. C is the 'core-wall only' system, CO is the 'core wall plus outrigger wall' system, CB is the 'core wall plus belt wall' system, and COB is the 'core wall plus outrigger wall plus belt wall' system. The outrigger and belt walls are installed only at the 15th and 30th floors and their thickness is

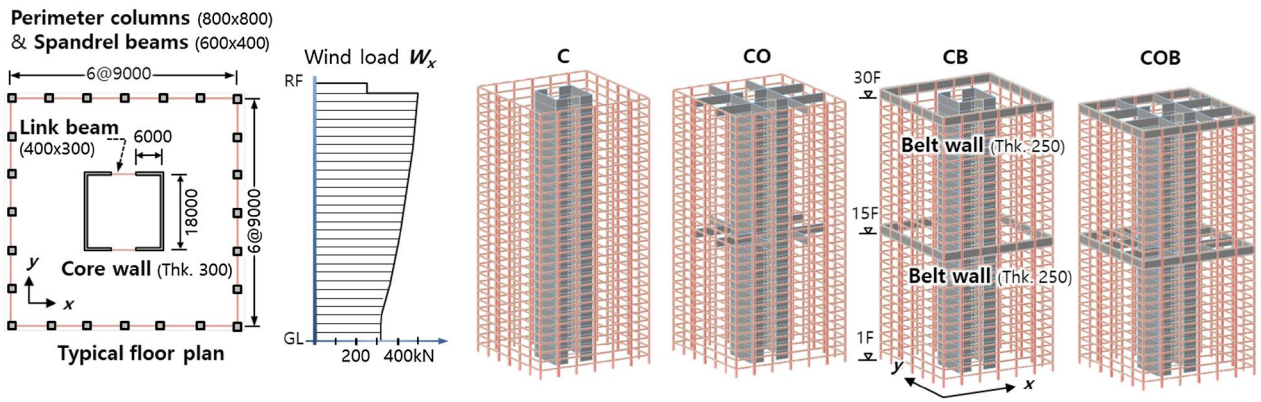

Fig. 3 Floor plan and structural systems of prototype concrete high-rise buildings considered for parametric study (mm).

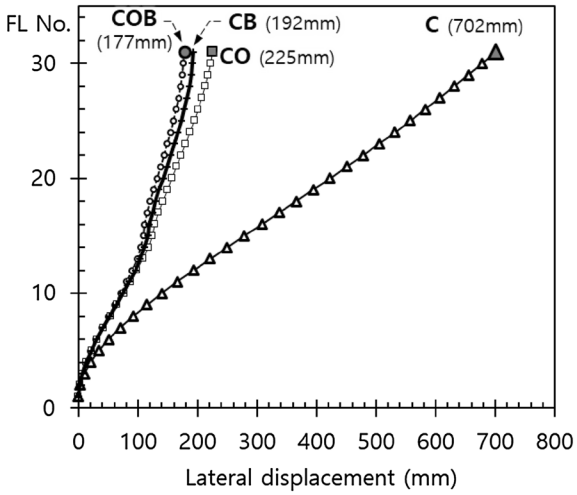

Fig. 4 Lateral displacements of conventional structure systems obtained by elastic analysis for W_x.

assumed as 250 mm. For structural analysis for lateral wind loads, the floor slab is considered as a strong diaphragm. The elastic modulus of concrete is assumed as $E_c = 27{,}000$ MPa. Since the purpose of this section is to make a comparative study of lateral resistance between different structural systems, only x-directional wind loads W_x are considered. The wind loads determined based on the basic wind velocity 30 m/s, $W_x = 319$–493 kN, are shown in Fig. 3.

Figure 4 shows the distributions of lateral displacements obtained from elastic analyses for W_x. Compared with the 'core wall only' system, the lateral displacements are significantly reduced in all the conventional systems with outrigger and/or belt walls (i.e. CO, CB, and COB). What is interesting in Fig. 4 is that the distribution of lateral displacements in CB is almost equivalent to that of COB. This indicates that, even if actual outrigger is not used, the belt walls acting as virtual outriggers are effective in reducing lateral displacement.

The force transfer mechanism of the belt walls as virtual outriggers in CB can be quantitatively evaluated by investigating difference in column axial forces at the 14th and 16th floors (i.e. column axial forces above and below the belt walls). For CB, as shown in Fig. 5a, the column axial forces above and below the belt walls are significantly different, which means a portion of the core wall moment is transferred to the perimeter columns through the belt walls. The difference in the column axial forces is significant not only at the corner columns but also at the adjacent intermediate columns placed along the y-direction. This indicates that by using the belt walls, the shear leg effect is alleviated. On the other hand, for C, as shown in Fig. 5b, the column axial forces are large only at the corners due to the shear lag effect, and the difference between the column axial forces above and below the belt walls is small.

2.2 Distributed Belt Wall System

The concept of the virtual outrigger effect, demonstrated in the previous section, can be extended further by distributing individual belt walls along the height of the building. Five distributed belt wall systems, CB1–CB5, are presented as an example in Fig. 6. Compared with CB with 48 individual belt walls (refer to Fig. 3), the number of individual belt walls used in CB1–CB5 is decreased to 24, 32, or 40. Figure 6 shows the lateral displacements of five distributed belt wall systems, each of which is the results of elastic analysis for the x-directional wind loads W_x in Fig. 3. The magnitude and distribution of the lateral displacements are different depending on the number and arrangement

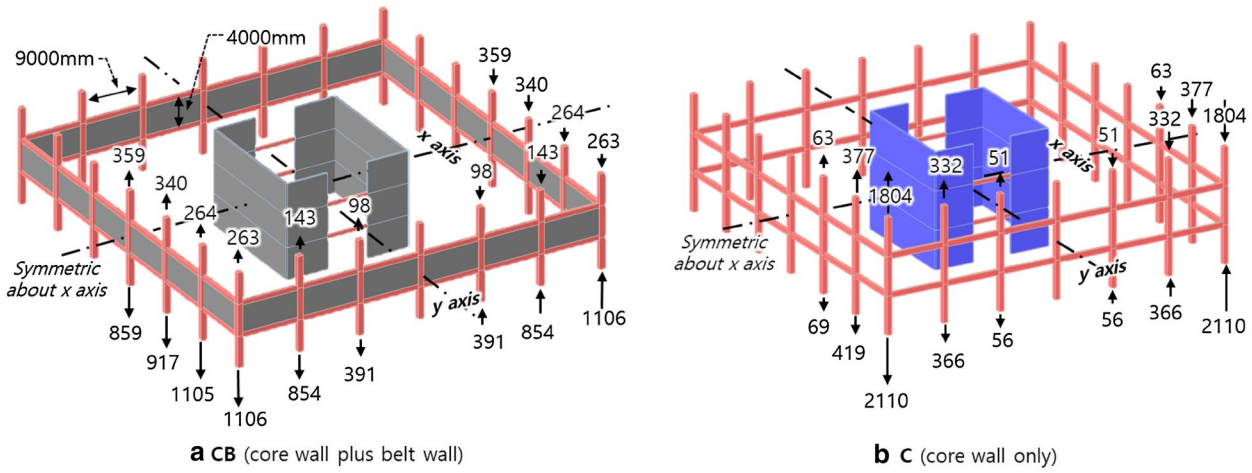

Fig. 5 Distribution of column axial forces above and beneath the 15th floor belt walls.

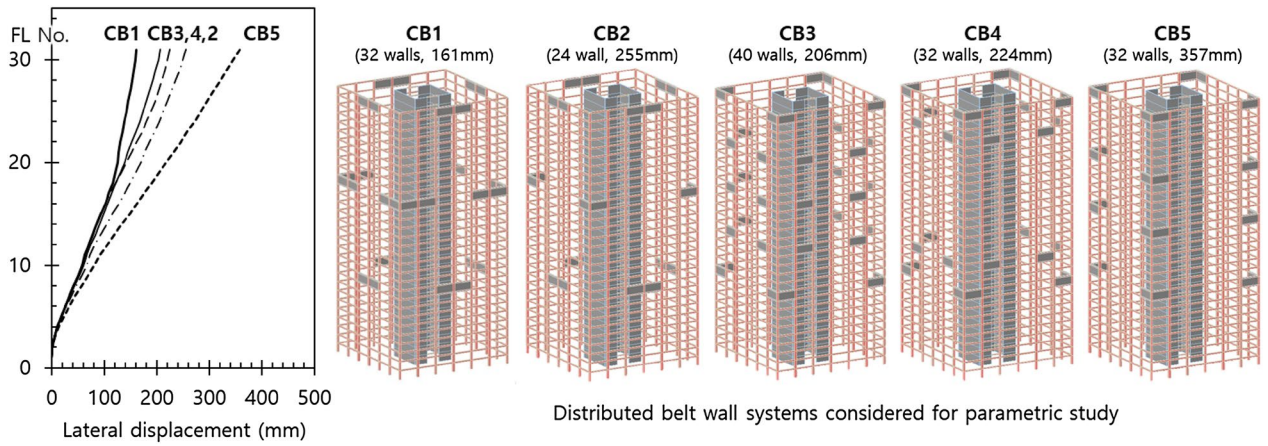

Fig. 6 Distributed belt wall systems as lateral force-resisting structure system of concrete high-rise buildings.

of the belt walls. Among the five distributed belt wall systems, the results of CB1 and CB3 are comparable to those of the conventional systems CO, CB, and COB (refer to Fig. 3). This indicates that the virtual outrigger effect works even in the case of placing the belt walls in isolation.

The force transfer mechanism between the core and individual belt walls in the distributed belt wall system is conceptually presented in Fig. 7. As shown in Fig. 7a, the horizontal shear force is transferred between the core wall and belt wall through the top and bottom floor slabs. When the core wall displaces laterally with a slope, the perimeter columns tied by the belt wall should displace laterally with the same slope, as shown in Fig. 7a2. Otherwise, the displacement compatibility is violated, as shown in Fig. 7a3. Consequently, such displacement compatibility induces large axial tension and compression forces to the perimeter columns tied to the belt walls.

The force transfer between the core and belt walls is presented in more detail in Fig. 7b. The horizontal shear force, V_u, is transferred from the core wall to the belt wall by the in-plane shear action of the top and bottom floor slabs. This horizontal shear force should be in moment equilibrium with a vertical shear force, V_v. Thus, by letting the horizontal and vertical dimensions of the belt wall l_w and h_w, respectively, the horizontal shear force V_u can be expressed as

$$V_u = V_v \frac{l_w}{h_w} \tag{1}$$

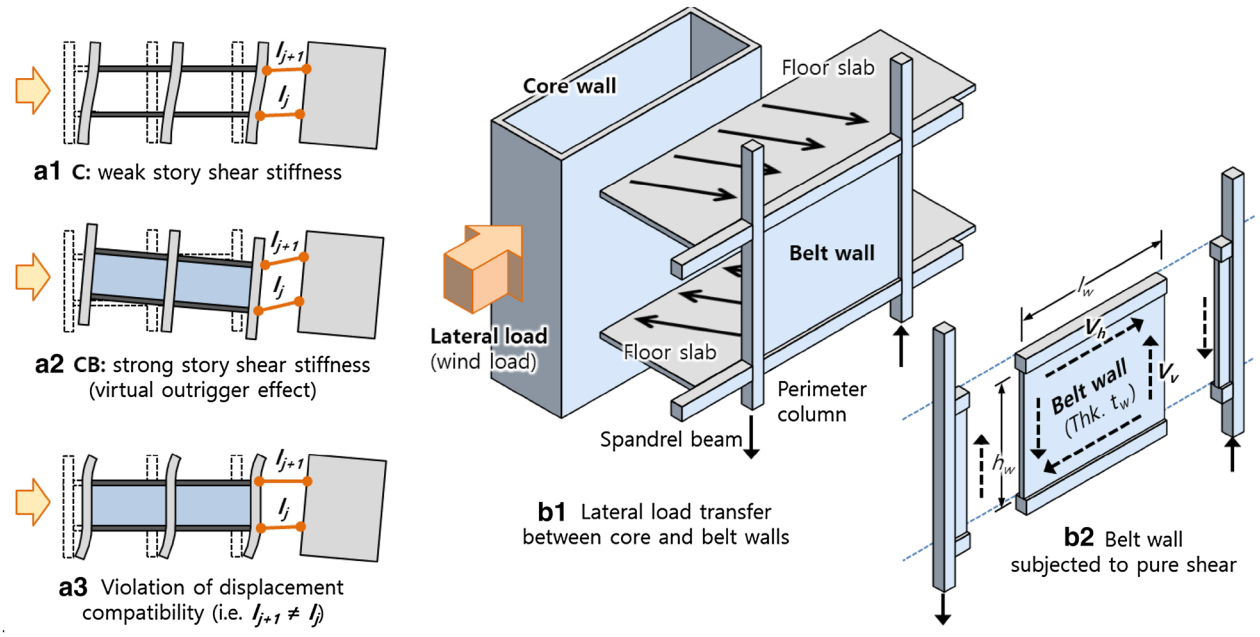

Fig. 7 Force transfer mechanism of distributed belt walls as virtual outrigger.

The horizontal and vertical shear forces, V_u and V_v, indicate that the belt wall is subjected to pure shear. In addition, since the vertical shear force V_v should be cancelled out by the reaction forces at the bottom of the boundary elements, a vertical axial force, which is equal to V_v, is induced to the perimeter columns. Such axial force is imposed as additional axial loads on the perimeter columns. This indicates that the shear demand of belt walls can be obtained by examining the axial forces acting on the upper and lower columns of the belt wall.

The distributed belt wall system as a lateral force-resisting system for high-rise buildings has advantages over the conventional concentrated belt wall systems as follows.

- Since only a portion of the building façade is covered by belt walls, restrictions on architectural planning at the floor where the belt walls are placed is alleviated.
- For the belt wall systems planned as virtual outriggers, the floor slabs are subjected to high in-plane shear demand. If the belt walls are concentrated at one floor, the shear force acting on the slabs increases significantly. The distributed belt wall system can be an alternative to reduce the high in-plane shear demand of the slabs.

3 Shear Strength of Belt Walls

As discussed in the previous section, the belt wall is subjected to pure shear. Thus, the conventional shear strength equations for structural walls subjected to combined bending and shear, such as $V_n = 0.17\sqrt{f_c'}bd + f_{yt}A_v d/s$, may not be directly used for the design of the belt walls (b and d = width and effective depth, respectively, and f_{yt} and s = yield strength and spacing of shear reinforcement, respectively). Furthermore, the shear stress level of the belt wall, defined as $\tau_u = V_u/[l_w t_w]$, is mostly higher than the allowable

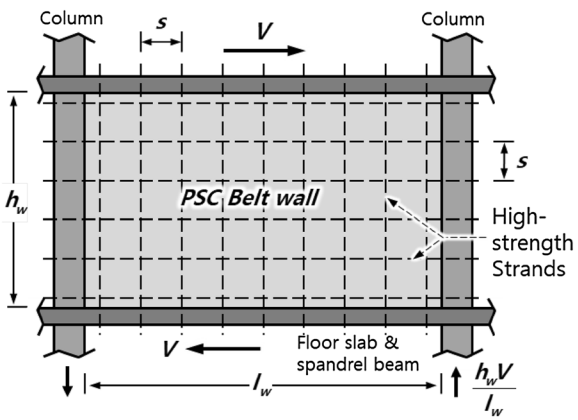

Fig. 8 Prestressed belt wall system.

maximum stress, $0.83\sqrt{f_c'}$, specified in concrete design codes such as ACI 318-14 and KCI 2012.

To address such high shear demand, in this study, it is proposed into use a prestressed concrete (PSC) system for the belt walls. Figure 8 shows a belt wall reinforced horizontally and vertically with high-strength strands. By tensioning the strands placed in both directions, it is possible to prevent concrete cracking from occurring early under lateral loading. After concrete cracking, the high-strength strands themselves act as a shear reinforcement for the belt wall. In the construction viewpoint, placement and tensioning of strands are not difficult because the belt walls are distributed separately.

In this section, the shear strengths of the proposed PSC belt walls at concrete cracking and reinforcement yielding are estimated based on the compression field theory as follows (Collins and Mitchell 1980; Vecchio and Collins 1986).

3.1 Material Models and Basic Assumptions

For the concrete, as shown in Fig. 9a, a linear elastic behavior following the elastic modulus E_c is adopted for design though the actual behavior is nonlinear. The tensile strength of the concrete, f_{ct}, is taken as $0.33\sqrt{f_c'}$ (Eom et al. 2018). For the high-strength prestressing (PS) strands, as shown in Fig. 9b, a bilinear behavior following the elastic modulus $E_{ps}=195$ GPa and post-yield modulus $E_{pp}=0.05E_{ps}$ is assumed. The yield and ultimate strengths of the PS strands are $f_{pu}=1860$ MPa and $f_{py}=1674$ MPa, respectively. For simple calculation, the behavior of the PS strands is idealized as a bilinear relationship and the yield strength f_{py} is taken as 90% of the ultimate strength (i.e. $f_{py}=0.9f_{pu}$, European Committee for Standardization 2004; Han et al. 2018; Lee et al. 2018).

The biaxial stresses and strains of the concrete are presented in Fig. 10. f_{cx} and f_{cy} are the normal stresses

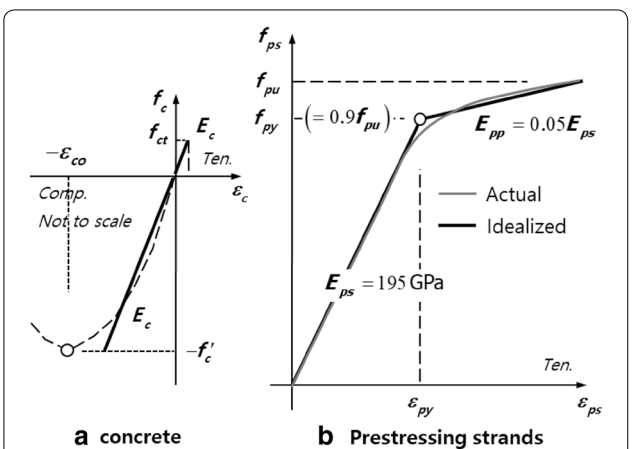

Fig. 9 Uniaxial behavior of concrete and PS strand for design.

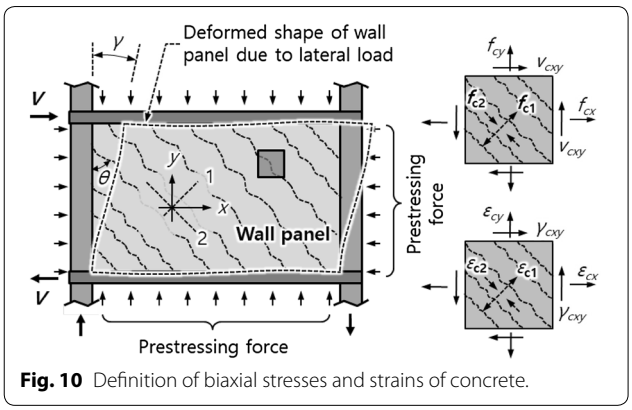

Fig. 10 Definition of biaxial stresses and strains of concrete.

acting along the x and y axes, respectively, and v_{cxy} is the shear stress. ε_{cx}, ε_{cy}, and γ_{cxy} are the concrete strains corresponding to f_{cx}, f_{cy}, and v_{cxy}, respectively. f_{c1}, ε_{c1}, f_{c2} and ε_{c2} are the concrete stresses and strains along the two principal directions. θ is the inclination angle of the principal direction. For the stresses and strains of the concrete, positive and negative signs indicates tension and compression, respectively. It is noted that only the $f_{c1}-\varepsilon_{c1}$ and $f_{c2}-\varepsilon_{c2}$ relationships follow the uniaxial behavior presented in Fig. 9a.

For simple formulation, basic assumptions regarding application of the compression field theory are made as follows.

- Since the belt wall is confined by the left and right perimeter columns and by the top and bottom floor slabs including spandrel beams, uniform stress and strain field is assumed for the internal concrete panel of the belt wall. Thus, the behavior of the concrete panel can be represented as the stresses and strains of an element, shown in Fig. 10.
- The PS strands are placed along the x and y axes as reinforcements. The spacing and cross-sectional area of the PS strands in both axes are the same. The prestressing force applied to each strand by post-tensioning is also the same as f_{pe}, where f_{pe} is the effective prestress. Based on these conditions, a constant inclination angle of the principal stresses, $\theta=45°$, is assumed.

In fact, the stresses and strains of the belt wall are not uniform because the confinement effects are different at the corner and center. Such local behavior is investigated further by nonlinear finite element analysis in the next section.

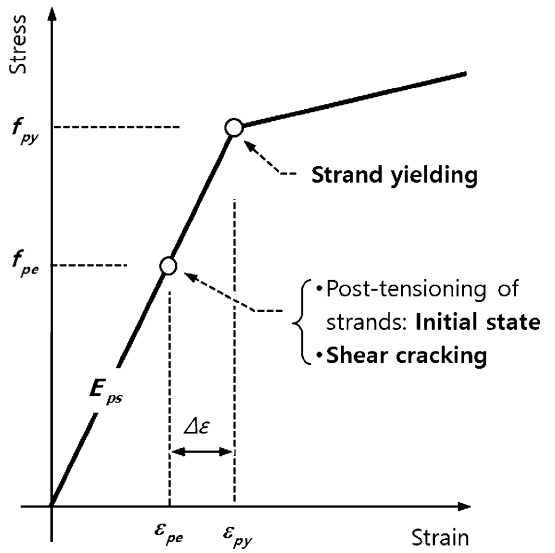

Fig. 11 Behavior of PS strands under post-tensioning and lateral loading.

3.2 Prestressing of Strands: Initial State

If the PS strands are post-tensioned to develop the effective prestress f_{pe}, as shown in Fig. 11, the concrete is compressed by an initial stress $f_{cx}=f_{cy}=f_{ci}$. By letting the reinforcement ratio of PS strands ρ_p, the initial stress and strain of the concrete, f_{ci} and ε_{ci}, respectively, can be expressed as

$$f_{ci} = -\rho_p f_{pe} \quad \text{and} \quad \varepsilon_{ci} = \frac{f_{ci}}{E_c} = -\frac{\rho_p f_{pe}}{E_c} \tag{2}$$

Since the concrete is compressed by the same f_{ci} both in the x and y axes, the biaxial stress and strain of the concrete is represented as a point, as shown in Fig. 12a1, a2.

3.3 Shear Cracking: Behavior of Uncracked Concrete

If a lateral shear force V is applied after the post-tensioning of the PS strands, the concrete panel of the belt wall is subjected to a pure shear stress, $v=V/[l_w t_w]$. Under the pure shear, the stress and strain circles of the uncracked concrete enlarge around the initial point (i.e. f_{ci} and ε_{ci}) with no change of their centers, as shown in Fig. 12b1, b2. Furthermore, since the inclination angle of the principal axis is $\theta=45°$, the normal stresses and strains remains constant as $f_{cx}=f_{cy}=f_{ci}$ and $\varepsilon_{cx}=\varepsilon_{cy}=\varepsilon_{ci}$. Then, when the principal stress in tension, f_{c1} $(=f_{ci}+v)$ reaches the tensile strength f_{ct}, shear cracking occurs in the belt wall. Thus, the shear stress and strain of the concrete at shear cracking, v_{cr} and γ_{cr}, can be computed as follows.

$$f_{ci} + v_{cr} = f_{ct} \quad \text{or} \quad v_{cr} = f_{ct} - f_{ci} = f_{ct} + \rho_p f_{pe} \tag{3}$$

$$\gamma_{cr} = 2\gamma_c = 2(\varepsilon_{ct} - \varepsilon_{ci}) = 2\left(\frac{f_{ct} + \rho_p f_{pe}}{E_c}\right) \tag{4}$$

where ε_{ct} is the cracking strain of the concrete, taken as f_{ct}/E_c.

Since the normal strains of the concrete remained constant as $\varepsilon_{cx}=\varepsilon_{cy}=\varepsilon_{ci}$, as shown in Fig. 12b2, the stress and strain of the PS strands do not change until the shear cracking occurs.

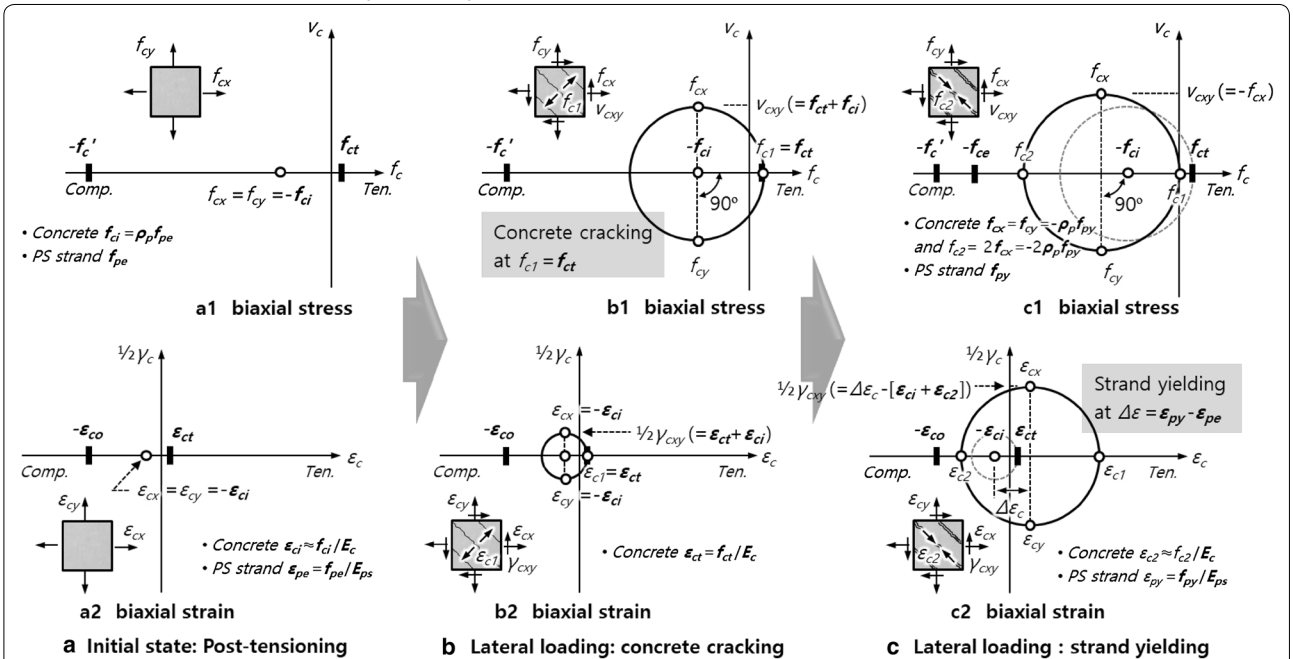

Fig. 12 Biaxial stresses and strains of concrete in wall concrete under post-tensioning and lateral loading.

3.4 Yielding of PS Strands: Behavior of Cracked Concrete

As the lateral force of the belt wall increases further after shear cracking, the tensile principal stress f_{c1} decreases to 0 and the compressive principal stress f_{c2} increases in magnitude (see Fig. 12c1). In addition, the concrete dilates as the width of shear cracks increase. Consequently, the normal strains of the concrete, ε_{cx} and ε_{cy}, increase from ε_{ci} in compression to a positive value in tension by $\Delta\varepsilon$, as shown in Fig. 12c2, and the strain of the PS strands also increase by the same amount, as shown in Fig. 11. In the end, it is considered that the yielding of the PSC belt wall occurs when the strain of the PS strands is equal to the yield strain, ε_{py} ($=f_{py}/E_{ps}$).

As shown in Fig. 10, there is no external load applied within the concrete panel of the belt wall. This means the confining force provided to the concrete by the PS strands (i.e. $-\rho_p f_{py}$) should be in equilibrium with the internal resultant force of the concrete (f_{cx} or f_{cy}). Thus, by taking the normal stresses of the concrete as $f_{cx}=f_{cy}=-\rho_p f_{py}$ and by letting the shear stress v_{cxy} be equal to f_{cx} or f_{cy} ($\theta=45°$, refer to Fig. 12c1), the belt wall shear stress at strand yielding, v_y, can be computed as

$$v_y = v_{cxy} = -f_{cx} = \rho_p f_{py} \tag{5}$$

As shown in Fig. 12c2, the shear strain of the belt wall at strand yielding, γ_y, can be computed as

$$\gamma_y = 2\gamma_c = 2(\Delta\varepsilon - \varepsilon_{c2} + \varepsilon_{ci}) \tag{6}$$

In Eq. (2), ε_{ci} is equal to $-\rho_p f_{pe}/E_c$. $\Delta\varepsilon$ is taken as $[\varepsilon_{py}-\varepsilon_{pe}]$ or $[f_{py}-f_{pe}]/E_{ps}$, as shown in Fig. 11. In addition, the compressive principal stress f_{c2} is equal to $2f_{cx}=-2\rho_p f_{py}$ (refer to Fig. 12c1), and thus ε_{c2} ($=f_{c2}/E_c$) can be approximated as $-2\rho_p f_{py}/E_c$. Therefore, Eq. (6) can be rewritten as

$$\gamma_y = 2\left(\frac{f_{py}}{E_{ps}}\left[1+2n_p\rho_p\right] - \frac{f_{pe}}{E_{ps}}\left[1+n_p\rho_p\right]\right) \tag{7}$$

where n_p is the elastic modulus ratio of the PS strands to concrete ($=E_{ps}/E_c$). γ_y estimated by Eq. (7) is based on the assumption that yielding of the PS strands precedes crushing failure of the concrete. Thus, the compressive principal stress f_{c2} (i.e. the compressive stress of diagonal concrete struts) should not exceed the effective compressive strength, $f_{ce}=0.85\beta_s f_c'$, specified in concrete design codes such as ACI 318-14 and KCI 2012.

$$|f_{c2}| = 2\rho_p f_{py} \le 0.85\beta_s f_c' \tag{8}$$

where β_s is the factor addressing the effects of cracking and reinforcements on the effective strength of the concrete strut.

3.5 Shear Strength of PSC Belt Walls

Multiplying v_{cr} and v_y by the cross-section area of the belt wall, $l_w t_w$, the belt wall shear strength at shear cracking and yielding, V_{cr} and V_y, respectively, are computed as.

$$V_{cr} = \left(f_{ct} + \rho_p f_{pe}\right) l_w t_w \tag{9}$$

$$V_y = \rho_p f_{py} l_w t_w \tag{10}$$

When designing the PSC belt walls, V_{cr} and V_y can be used for strength check such as the serviceability and ultimate limit states. In this case, the horizontal shear force of the belt wall, V_u, transferred via the floor slab should not exceed ϕV_{cr} or ϕV_y ($\phi=0.75$).

As shown in Eq. (9), the effective prestress and reinforcement ratio of the PS strands, f_{pe} and ρ_p, need to be increased to secure a greater resistance against shear cracking under service loads. However, excessively large f_{pe} and ρ_p are not desirable for the design of belt walls because brittle failure such as crushing of concrete strut can occur. Thus, when post-tensioning the PS strands used for the belt walls, the effective prestress and reinforcement ratio of the PS strands, f_{pe} and ρ_p, should be limited as follows.

- In the viewpoint of practical application, the shear cracking strength V_{cr} might not be greater than the shear yield strength V_y. By taking $V_y \ge V_{cr}$ in Eqs. (9) and (10), the effective prestress f_{pe} is limited to

$$f_{pe} \le f_{py} - \frac{f_{ct}}{\rho_p} \tag{11}$$

- To prevent early concrete crushing, the compressive stress f_{c2} of diagonal concrete struts should not exceed the effective compressive strength f_{ce}, as discussed in Eq. (8). Thus, if the factor β_s is taken as 0.6 in Eq. (8) for conservative design, the reinforcement ratio ρ_p is limited to (ACI 318-14 and KCI 2012)

$$\rho_p \le 0.51\frac{f_c'}{f_{py}} \tag{12}$$

4 Nonlinear Finite Element Analysis

To investigate the behavior of PSC belt walls proposed to use as virtual outriggers in concrete high-rise buildings, finite element (FE) analysis was performed. For the FE modeling and analysis, VecTor2 developed by Prof. F. J. Vecchio in University of Toronto was used (Wong et al. 2013). VecTor2, which is based on the modified compression field theory (Vecchio and Collins 1986), is suitable for analyzing 2-dimensional structures under biaxial stresses, such as shear walls.

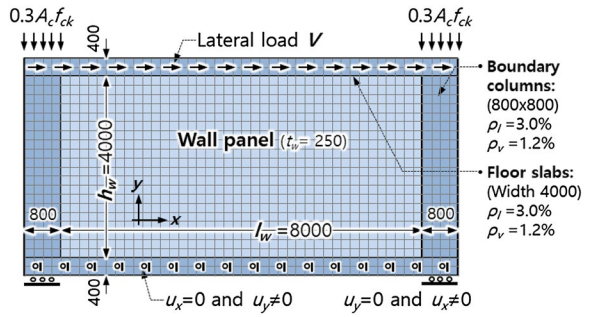

Fig. 13 PSC belt wall specimen for finite element analysis (mm).

4.1 Finite Element Modeling and Material Behaviors

Figure 13 shows the dimensions and reinforcement details of the PSC belt wall specimen used for the analysis. The belt wall consists of the left and right boundary columns, top and bottom floor slabs, and wall panel. The wall panel is $l_w = 8000$ mm long and $h_w = 4000$ mm high, and its thickness is $t_w = 250$ mm. The section size of the boundary columns is 800 mm × 800 mm. The section size of the top and bottom slabs is 400 mm deep and 4000 mm wide. The section width of the slabs is assumed as sufficiently large, considering the contributions of spandrel beams. The compressive strength, tensile strength, and elastic modulus of the concrete used in the belt wall are $f_c' = 40$ MPa, $f_{ct} = 0.33\sqrt{f_c'} = 2.09$ MPa, and $E_c = 30{,}000$ MPa. In the boundary columns and slabs, the reinforcement ratios of longitudinal and transverse steel bars are $\rho_l = 3.0\%$ and $\rho_v = 1.2\%$, respectively. The yield strength of the reinforcing steel bars used for the columns and slabs is $f_y = 400$ MPa. In the wall panel, high-strength PS strands of $f_{pu} = 1860$ MPa are used along the horizontal and vertical directions.

Figure 13 shows the mesh discretization of the belt wall. The bilinear rectangular element of mesh size 200 mm × 200 mm is used to model the plane concrete of the wall panel and boundary columns and slabs. The steel reinforcements used in the boundary columns and slabs are modeled as smeared reinforcement elements. On the other hand, the PS strands reinforcing the wall panel are modeled as uniaxial line elements placed horizontally and vertically with the same spacing 200 mm. To consider the behavior of unbonded PS strands, the line elements representing the PS strands and the plane elements representing the concrete panel share nodes only at the four boundaries of the wall panel.

As shown in Fig. 13, the loading and support conditions of the belt wall are applied as close to those in Fig. 7b as possible. First, the lateral load of the belt wall is applied to the top slab as a uniform line loading along the slab length, while horizontal displacements of the bottom slab are constrained ($u_x = 0$ and $u_y \neq 0$). Second, the axial compression force 7680 kN, which is equivalent to $0.3f_c'$ in stress, is applied to the top of the columns. At the bottom, on the other hand, vertical displacements are constrained ($u_x \neq 0$ and $u_y = 0$).

The stress–strain relationships of the concrete in tension and compression are modeled as the parabolic–linear model embedded in VecTor2 (Wong et al. 2013). Confinement effects by biaxial compression, such as strength and ductility enhancement, are not considered. On the other hand, decrease in the compressive strength of concrete strut due to transverse tensile cracks (i.e. compression softening), occurring under the biaxial state of tensile and compressive stresses, is taken into account as the effective compressive strength f_{ce} (Vecchio and Collins 1986). For steel reinforcements used in the boundary columns and slabs, the linear strain-hardening model is used. Bar buckling is not considered. For the high-strength PS strands, a bilinear model following the elastic modulus $E_{ps} = 195$ GPa and post-yield modulus $E_{pp} = 0.05E_{ps}$ is used (refer to Fig. 9b). The effective prestress applied to the PS strands, f_{pe}, is considered by adjusting the initial strain.

4.2 Results of FE Analysis

Four belt wall specimens PT23V, PT26V, PT43V, and PT46V are considered for the FE analysis. The design parameters considered are the effective prestress and reinforcement ratio of PS strands, f_{pe} and ρ_p, respectively. The values of f_{pe} and ρ_p used in each specimen are shown in Table 1. The allowable maximum values of f_{pe} and ρ_p, computed from Eqs. (11) and (12), are also presented in the table. In all specimens, the reinforcement ratios of PS strands are 0.2% and 0.4%, which are less than the allowable maximum value, 1.22%. For PT26V, the effective prestress $f_{ce} = 0.629f_{pu}$ is significantly greater than the allowable maximum value, $0.338f_{pu}$.

Figure 14 shows the lateral force–displacement (V–Δ) relationships by FE analyses. For comparison, the shear cracking and yield points predicted by the proposed method are also represented as triangles. Overall, the

Table 1 Design parameters of PSC belt wall specimens.

Specimen	Effective prestress f_{pe}	$f_{pe,max}$[a]	Reinforcement ratio ρ_p (%)	$\rho_{p,max}$ (%)[b]
PT23V	$0.315f_{pu}$	$0.338f_{pu}$	0.2	1.22
PT26V	$0.629f_{pu}$	$0.338f_{pu}$	0.2	1.22
PT43V	$0.315f_{pu}$	$0.623f_{pu}$	0.4	1.22
PT46V	$0.629f_{pu}$	$0.623f_{pu}$	0.4	1.22

[a] $f_{pe,max}$ is taken as $[f_{py} - f_{ct}/\rho_p]$ from Eq. (11).

[b] $\rho_{p,max}$ is taken as $0.51f_c'/f_{py}$ from Eq. (12).

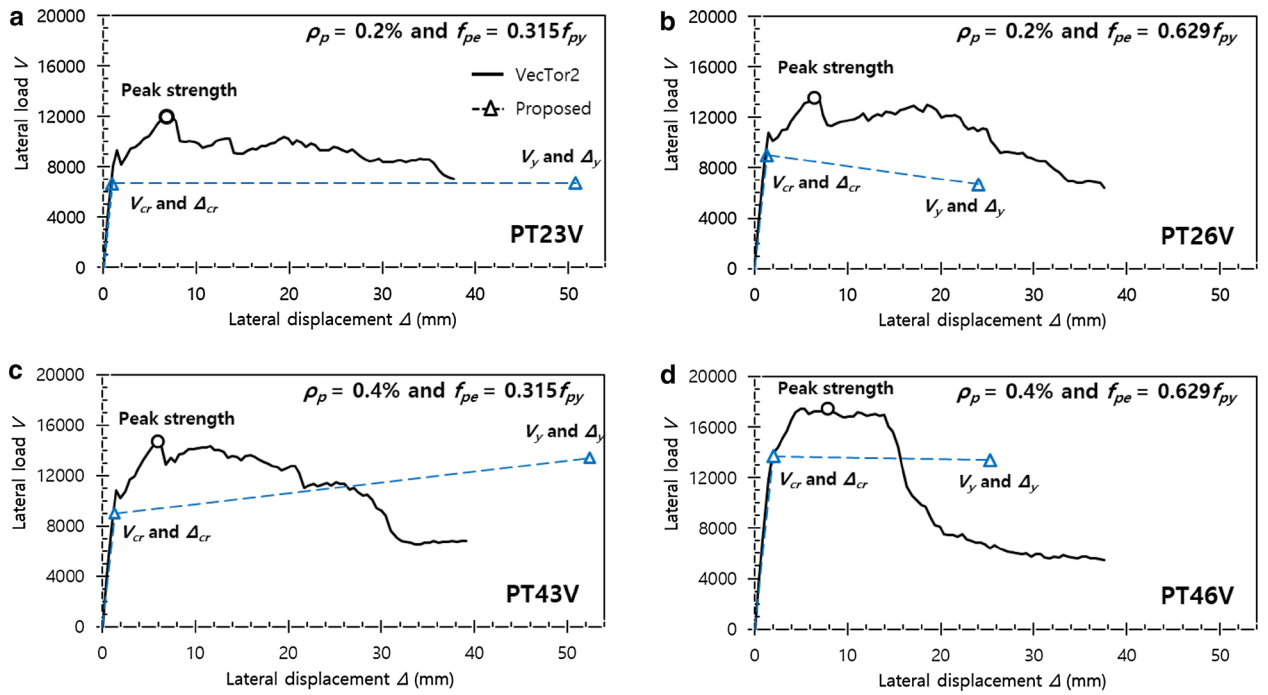

Fig. 14 Lateral load–displacement relationships by FE analysis.

V–Δ behavior by the FE analysis is similar in all specimens. The initial stiffness of the belt walls is very high. The stiffness decreases at $\Delta = 1$–2 mm as diagonal shear cracks occur in the wall panel. At the onset of diagonal shear cracking, the belt wall strength decreases slightly because the tensile stress of the concrete is rapidly released, but bounces back shortly. In all specimens, the peak strength occurs at $\Delta = 6$–8 mm. After the peak strength, a strength-degradation behavior occurs in all specimens as the crack width at the wall panel increases significantly.

In Fig. 15a, the distribution of concrete principal stresses f_{c2} at the peak strength is represented as the dark contour. In Fig. 15b, the distributions of deformations and cracks occurring at the peak strength are presented. The diagonal concrete struts forming in the wall panel along the 45° line are clearly seen in the figure. The vertical component of the strut compression force pushes up and down the boundary slabs, and consequently the belt wall swells up and down at the center and the width of shear cracks increases. The increase in the crack width accelerates compression softening of the concrete strut, which is responsible for the post-peak strength degradation of the belt walls.

Figure 16 shows the normal and shear stresses of concrete, f_{cx}/f_{cy} and v_{cxy}, occurring along the boundaries of the wall panel in PT46V. At the vertical boundaries to the left and right columns, the normal stress of concrete is f_{cx}. On the other hand, at the horizontal boundaries to the top and bottom slabs, the normal stress of concrete is f_{cy}. The concrete stresses occurring at the points of shear cracking (i.e. $\Delta = 2.0$ mm) and peak strength (i.e. $\Delta = 7.8$ mm) are presented in Figs. 15b and 16a, respectively. At the onset of shear cracking, v_{cxy} is distributed almost uniformly at all boundaries, as shown in Fig. 16a. This is consistent with the uniform stress field assumption used for the formulation of V_{cr} and V_y. On the other hand, at the point of peak strength, v_{cxy} is not uniformly distributed, but concentrated at the corners and along the diagonal struts, as shown in Figs. 15d1 and 16b. This indicates that, after the shear cracking of the belt wall occurs, the predictions based on the uniform stress and strain field might be inaccurate.

4.3 Comparison of Belt Wall Shear Strengths

In Fig. 14, the belt wall shear strengths V_{cr} and V_y, computed by Eqs. (9) and (10), respectively, are compared with the V–Δ relationships obtained by the FE analysis. The lateral displacements Δ_{cr} and Δ_y, computed by multiplying γ_{cr} and γ_y by the center-to-center height of the belt wall ($h_w = 4400$ mm), are also compared (refer to the dashed lines). V_{cr} and Δ_{cr} at shear cracking are in good agreement with the results of FE analyses in all specimens, despite different f_{pe} and ρ_p. On the other hand, V_y and Δ_y at shear yielding are significantly different from the post-cracking behavior by the FE analysis.

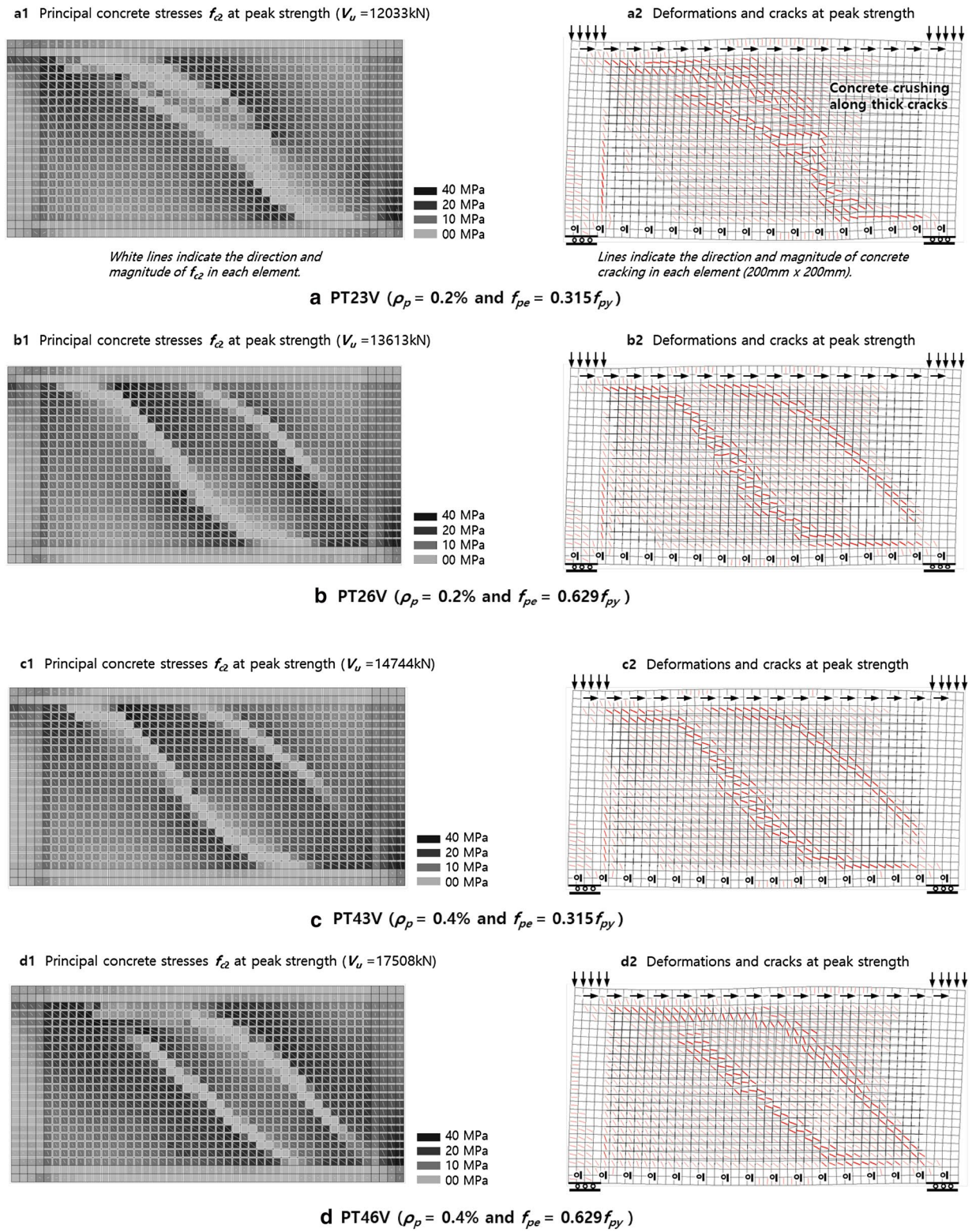

Fig. 15 Distributions of concrete stress, deformation, and cracks by FE analysis.

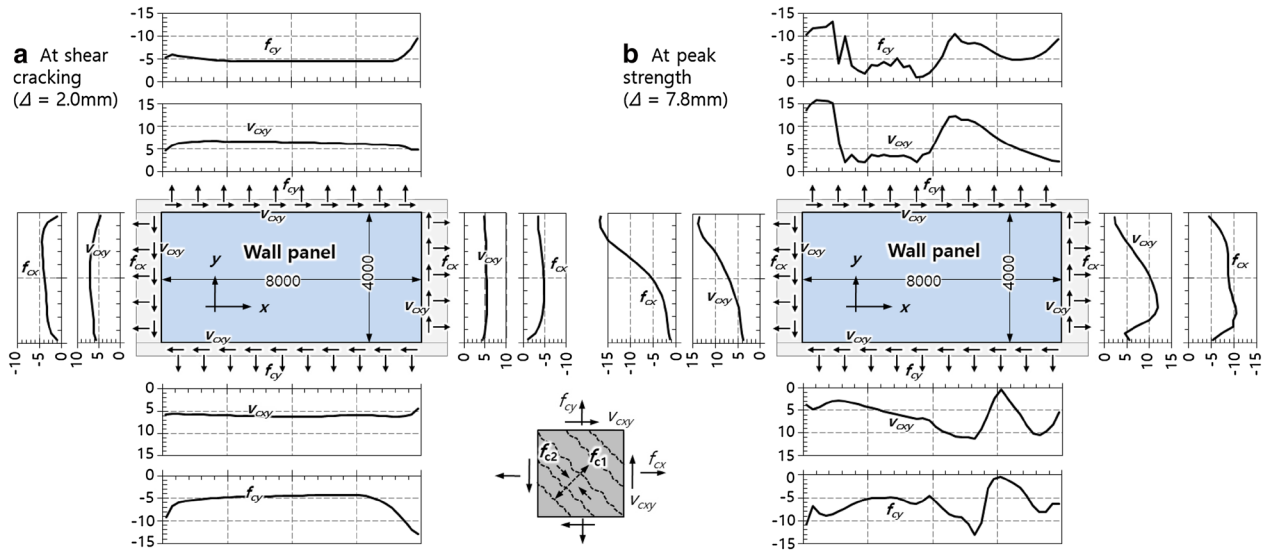

Fig. 16 Distributions of concrete stresses along the boundaries of belt wall panel (PT46V).

This is because after shear cracking, the distribution of concrete stresses and strains in the wall panel become highly non-uniform, as shown in Figs. 15 and 16, and thus the compression field theory based on uniform stress and strain field does not work well.

As shown in the V–Δ relationships of PT23V and PT26V obtained by FE analyses, the belt wall shear strength at shear cracking increases with increasing effective prestress f_{pe}. In addition, as seen from the comparison of the V–Δ relationships between PT23V and PT43V, the shear strength of the belt wall increases with increasing reinforcement ratio ρ_p. These trends are explained well from the equation of V_{cr} in Eq. (9).

In all specimens, the peak strength by the FE analysis is greater than V_y, although the PS strands do not reach their yield strength at the peak strength. The belt wall shear strength greater than V_y is attributed to the contribution of the boundary columns. In PT46V, for example, the shear strength contributed by the internal wall panel, computed by integrating v_{cxy} at the bottom shown in Fig. 16b, is only 12,494 kN, which is less than $V_y = 13{,}392$ kN. Only after the shear strengths provided by the left and right boundary columns, 1340 and 3732 kN, respectively, are added, the belt wall shear strength in total (= 17,508 kN) is greater than V_y.

5 Design Recommendation

When designing the PSC belt walls used as virtual outriggers in high-rise buildings, elastic design is desirable based on the shear strength V_{cr}. As shown in Eq. (9), early inclined cracking occurring in the wall panel subjected to high shear demand (i.e. pure shear) can be effectively restrained by adjusting the effective prestress and reinforcement ratio of PS strands, f_{pe} and ρ_p. However, to prevent brittle failure, limitations on f_{pe} and ρ_p, defined in Eqs. (11) and (12), should be satisfied.

6 Summary and Conclusions

In this study, the force transfer mechanism of the distributed belt walls, used as virtual outriggers in concrete high-rise buildings, was investigated. For the reinforcement of the belt walls under high shear demand, a reinforcing method using high-strength PS strands was suggested, and the shear strength of the PSC belt walls was estimated based on the compression field theory. By performing nonlinear FE analysis, the shear behavior of the PSC belt walls was evaluated in detail. The conclusions of this study are as follows.

1. For the distributed belt wall system, the belt walls, without direct connection to the core wall and acting as virtual outriggers, are as effective in reducing lateral drift of the high-rise building as the conventional belt and outrigger structures are. The performance of the distributed belt wall system depends on the number and arrangement of belt walls.
2. Since the belt walls as virtual outriggers in high-rise buildings are subjected to pure shear, the existing shear strength equations based on flexure-shear

cracking failure might not be applicable. Instead, the shear strengths of the belt walls, such as cracking and yield strengths, should be based on the belt wall panel behavior under pure shear.

3. The belt walls can be reinforced with high-strength prestressing strands to meet high shear demand. In this case, the belt wall shear strength at the onset of inclined shear cracking, estimated by the compression field theory based on uniform stress and strain field, is in good agreement with the results of FE analyses. By increasing the effective prestress and reinforcement ratio of PS strands, the shear resistance of the PSC belt wall can be enhanced.
4. The results of the FE analysis show that the shear behavior of the PSC belt walls is with limited ductility and fails before reinforcement yielding. This is because, as the width of inclined shear cracks increase in the wall panel, the concrete stress are concentrated locally at the corner areas and along the diagonal struts. Thus, it is recommended that the shear design of the PSC belt walls be based on the cracking strength.

In addition to the analytical investigations, the performance of the proposed PSC belt wall system should be experimentally verified in the future. Particularly for a possible application to seismic design, the behavior of the belt wall under cyclic loading should be investigated further.

Authors' contributions

TSE contributed to writing the manuscript as the principle author. He derived design formula based on the compression filed theory, and investigated the detailed behavior of prestressed concrete belt walls through performing nonlinear finite element analysis. HM contributed to the numerical investigations of the prototype high-rise building. WY contributed to writing and reviewing the manuscript. His suggestions and comments improved the completeness and readability of the manuscript. All authors read and approved the final manuscript.

Author details

[1] Dept. of Architectural Engineering, Dankook Univ., 152 Jukjeon-ro, Yongin-si, Gyeonggi-do 448-701, South Korea. [2] Engineering, Procurement, and Construction Teem, SEN ENG. Group, SENSE B/D Beodeunaru-ro 19-gil 6, Youngdeungpo-gu, Seoul 07226, South Korea. [3] College of Civil Engineering, Hunan Univ., Lushan Road (S), Yuelu District, Changsha 410082, Hunan, China.

Acknowledgements

This research was supported by research grants funded by the Ministry of Land, Infrastructure, and Transport of Korea (Code 18AUDP-B106327-04, Architecture & Urban Development Research Program), and by National Natural Science Foundation of China (No. 51338004).

Competing interests

The authors declare that they have no competing interests.

Availability of data and materials

Not applicable.

Funding

Research grant funded by the Ministry of Land, Infrastructure, and Transport of Korea (Code 18AUDP-B106327-04, Architecture & Urban Development Research Program). Research grant funded by National Natural Science Foundation of China (No. 51338004).

Publisher's Note

Received: 17 August 2018 Accepted: 3 October 2018
Published online: 03 January 2019

References

ACI Committee 318. (2014). *Building code requirements for structural concrete (ACI 318-14) and commentary*. Farmington Hills, MI: American Concrete Institute.

Choi, H. S., & Joseph, L. (2012). Outrigger system design considerations. *International Journal of High-Rise Buildings, 1*(3), 237–246.

Collins, M. P., & Mitchell, D. (1980). Design proposals for shear and torsion. *Journal of the Prestressed Concrete Institute, 25*(5), 70.

Dean, B., Martin, O., Emery, D., & Chancellor, P. (2001). Tall building design innovations in Australia. In *Tall buildings and urban habitat, cities in the third millennium, 6th world congress of the council on tall buildings and urban habitat* (pp. 393–394). Melbourne: Planning and Architecture.

Eom, T.-S., Hwang, I.-H., Lee, S.-J., & Park, T.-W. (2018). Failure mode and shear strength of nonprestressed hollow-core slabs in one-way shear. *ACI Structural Journal, 115*(4), 1131–1141.

Eom, T.-S., Kim, J.-Y., Kim, J.-Y., Kim, J.-Y., & Kim, T.-Y. (2013). Shear design of concrete belt walls reinforced with post-tensioning strands. *Journal of Korean Society of Hazard Mitigation, 13*(1), 31–39.

European Committee for Standardization. (2004). *Eurocode2: Design of concrete structures—Part 1-1: General rules and rules for buildings. BS EN 1992-1-1: 2004*. London: British Standards Institute.

Han, S.-J., Lee, D. H., Oh, J.-Y., Choi, S.-H., & Kim, K. S. (2018). Flexural Responses of Prestressed Hybrid Wide Flange Composite Girders. *International Journal of Concrete Structures and Materials*, *12*(5), 581–596.

Korean Concrete Institute. (2012). *Design code for concrete structures (KCI-2012), 2012*. Seoul: Korean Concrete Institute.

Lee, D. H., Han, S.-J., Joo, H.-E., & Kim, K. S. (2018). Control of Tensile Stress in Prestressed Concrete Members Under Service Loads. *International Journal of Concrete Structures and Materials*, *12*(4), 453–469.

Midas, I. T. (2006) *Midas/Gen: General structural design system for windows, online manual, V.7.1.1 (R2)*, Korea.

Nair, R. S. (1998). Belt trusses and basement as "virtual" outrigger for tall buildings. *Engineering Journal American Institute of Steel Construction, 35*(4), 140–146.

Stafford Smith, B., Cruvellier, M., Nollet, M.-J., & Mahyari, A. T. (1996). Offset outrigger concept for tall buildings, tall building structures—A world view. In *Council on tall buildings and urban habitat* (pp. 73–80).

Vecchio, F. J., & Collins, M. P. (1986). The modified compression-field theory for reinforced concrete elements subjected to shear. *ACI Structural Journal, 83*(2), 219.

Wong, P. S., Vecchio, F. J., & Trommels, H. (2013). *VecTor2 & formworks user's manual* (2nd ed.). Toronto: University of Toronto.